
REVISIT, EXTEND, AND ENHANCE HESSIAN-FREE INFLUENCE FUNCTIONS

Ziao Yang^{† *}, Han Yue^{† *}, Jian Chen[‡], and Hongfu Liu[†]

Brandeis University[†], Tsinghua University[‡]

{ziaoyang,hanyue,hongfuliu}@brandeis.edu[†], chenj@sem.tsinghua.edu.cn[‡]

ABSTRACT

Influence functions serve as crucial tools for assessing sample influence in model interpretation, subset training set selection, noisy label detection, and more. By employing the first-order Taylor extension, influence functions can estimate sample influence without the need for expensive model retraining. However, applying influence functions directly to deep models presents challenges, primarily due to the non-convex nature of the loss function and the large size of model parameters. This difficulty not only makes computing the inverse of the Hessian matrix costly but also renders it non-existent in some cases. Various approaches, including matrix decomposition, have been explored to expedite and approximate the inversion of the Hessian matrix, with the aim of making influence functions applicable to deep models. In this paper, we revisit a specific, albeit naive, yet effective approximation method known as TracIn. This method substitutes the inverse of the Hessian matrix with an identity matrix. We provide deeper insights into why this simple approximation method performs well. Furthermore, we extend its applications beyond measuring model utility to include considerations of fairness and robustness. Finally, we enhance TracIn through an ensemble strategy. To validate its effectiveness, we conduct experiments on synthetic data and extensive evaluations on noisy label detection, sample selection for large language model fine-tuning, and defense against adversarial attacks.

1 Introduction

Data-centric learning is an emerging topic focusing on enhancing algorithmic performance from the perspective of training data [1] and aims to address data quality issues coupled with learning algorithms. In contrast to model-centric learning, which designs novel algorithms or optimization techniques for performance improvement with fixed training data, data-centric learning operates with a fixed learning algorithm while modifying the training data through trimming, augmenting, or other methods aligned with improving utility. Data-centric learning holds significant potential in many areas such as model interpretation, subset training set selection, data generation, noisy label detection, active learning, domain adaptation, fairness machine learning, and others [2, 3].

As the foundation of data-centric learning, influence estimation and data valuation approaches can be generally categorized into two categories [4]. (a) Retraining-based methods include the classical leave-one-out influence approach [5] retraining models and observing performance changes after removing one (or a group of) training sample(s). While useful as an ideal baseline, even on computation non-extensive models this is computationally untenable. Other representative methods such as model-agnostic Shapley value approaches [6, 7, 8] also suffer similar problems. Computationally efficient approaches such as KNN-Shap [9] tend to make assumptions about the learning model and hence are not directly applicable to other models being considered. (b) Gradient-based methods can be used to approximately estimate influence without expensive overheads of retraining. The seminal work in this category is that of [10], which utilizes a Taylor-series approximation and LiSSA optimization [11] to compute sample influences. However, the limiting assumption is that the model and loss function are convex. Despite debates on the necessity of convexity [12, 13, 14, 15], challenges persist when directly applying gradient-based methods to large models. The size of model parameters complicates calculations, particularly in obtaining the inverse of the Hessian matrix. Efforts,

*Equal contribution

including matrix decomposition techniques [10, 13, 3], aim to expedite and approximate Hessian matrix inversion, therefore enhance the feasibility of influence functions for deep learning models.

Contributions. In this paper, we revisit a particular naive yet aggressive approximation method TracIn [16] by substituting the inverse of the Hessian matrix with an identity matrix, representing it as the Hessian-free influence function, the inner product of the gradient of the validation set and the gradient of the sample under evaluation, which we term Inner Product (IP). We summarize our major contributions as follows:

- We redefine the TracIn method into IP formulation and delve into the rationale behind this simple yet effective approximation, offering insights into why it performs well in practical scenarios.
- Expanding on the TracIn framework, we extend its applicability beyond measuring sample influence on model utility to encompass considerations of fairness and robustness.
- To enhance the generalization of TracIn, we propose IP Ensemble, a novel approach leveraging dropout mechanisms to simulate diverse models. IP Ensemble amalgamates IP scores from these varied models, thus increasing the method’s generalization capabilities.
- We validate the effectiveness of IP through synthetic data experiments and conduct extensive real-world evaluations using IP Ensemble. These experiments span various applications, including noisy label correction for vision data, data curation aimed at fine-tuning fairer NLP models, and defense strategies against adaptive evasion adversaries.

2 Related Work

In this section, we introduce the literature on influence functions, with a focus on the acceleration of the calculation of the inverse of Hessian matrix, followed by various applications and miscellaneous.

Efficient Influence Estimation. Influence functions serve as crucial tools for estimating the individual valuation of data without requiring model retraining. However, the computation of the inverse of the Hessian matrix poses challenges for large-scale data and models. To address this issue, various approaches have been proposed to simplify or estimate the inverse of the Hessian matrix effectively. A seminal work in this domain is that of [10], which employs a Taylor-series approximation and LiSSA optimization [11] to compute sample influences. Similarly, EKFAC [13] enhances K-FAC by offering a more precise Hessian approximation through efficient eigendecomposition and managing damped inverse Hessian-vector products. More recently, DataInf [3] efficiently computes influence even for large models by replacing the inverse Hessian computation with a readily computable closed-form expression, although their framework may suffer from significant theoretical errors. TracIn [16], a straightforward yet aggressive approximation, substitutes the inverse of the Hessian matrix with an identity matrix, essentially considering gradients directly as a measure of influence. Beyond the conventional influence function that gauges sample influence on the validation set, self-influence [17, 18] computes influence using the training set alone.

Various Applications of Influence Functions. With the above efficient approximation, influence functions have diverse applications. One major application is identifying detrimental samples [19]. The learning performance can be further improved by removing [2], relabeling [20], or reweighting [18] the identified detrimental samples, which has significant implications in various fields such as noisy label detection [21], subset selection [22], and the identification of the most influential samples [23, 24]. Other applications encompass few-shot learning [25], where influence functions help improve model performance with minimal data, and recommendation systems [26, 27], enhancing the accuracy and personalization of recommendations. Influence functions are also valuable in selecting data for active learning [28], fairness machine learning [29, 30, 31], adversarial attack [32], graph machine learning [33, 34], machine unlearning [35, 36], out-of-distribution generalization [37], data privacy [38], domain adaptation [39], to name a few.

Miscellaneous. Several studies have examined the fragility of influence functions in explaining deep learning model predictions. [12] breaks down the difference between influence function estimates and leave-one-out retraining in neural networks into five factors, discovering that while influence estimates may not perfectly align with leave-one-out retraining, they approximate the proximal Bregman response function, offering valuable insights for identifying influential or mislabeled examples. [14] demonstrates that the effectiveness of influence functions in neural networks varies with network architecture, depth, width, parameterization, and regularization, underscoring their fragility in deep learning due to non-convex loss functions. [15] suggests that the instability of current validation procedures, rather than non-convexity or lack of regularization, may be responsible for their unreliability. Other topics include [40] expands influence functions from estimating the effects of removing one point to large groups of training samples; generalized influence functions [41] enhance influence estimation in large-scale models by concentrating on target parameters and addressing computational instability with a robust inverse-Hessian-vector product approximation; multi-stage influence function [42] extends traditional influence functions to monitor the impact of pre-training data on fine-tuned model predictions, facilitating the identification of crucial pre-training examples.

3 Methods

In this section, we introduce the preliminaries of the influence function, with a focus on the Hessian-free approximation, then elaborate on our extension and upgrade.

Revisit. Given a training set $T = \{z_i = (x_i, y_i)\}_{i=1}^n$ and a classifier trained using empirical risk minimization by a convex loss function ℓ , the optimal parameters of the classifier can be obtained by $\hat{\theta} = \arg \min_{\theta \in \Theta} \frac{1}{n} \sum_{i=1}^n \ell(z_i; \theta)$. To measure the impact of an individual data sample, we can train the model with and without the specific sample and see the performance change. However, the retrain-based approach is expensive for large-scale data and models. To avoid model retraining, influence functions estimate the effect of changing an infinitesimal weight of samples on a validation set $V = \{z_j = (x_j, y_j)\}_{j=1}^{n'}$, based on an impact function f evaluating the quantity of interest. If we measure the sample impact on model utility, i.e., the loss on the validation set, by removing this sample from the original training set, the sample influence can be estimated as follows [10]:

$$\mathcal{I}^{\text{util}}(-z_i) = \sum_{z_j \in V} \nabla_{\hat{\theta}} \ell(z_j; \hat{\theta})^T \mathbf{H}_{\hat{\theta}}^{-1} \nabla_{\hat{\theta}} \ell(z_i; \hat{\theta}), \quad (1)$$

where $\mathbf{H}_{\hat{\theta}} = \sum_{i=1}^n \nabla_{\hat{\theta}}^2 \ell(z_i; \hat{\theta})$ is the Hessian matrix of the convex ℓ loss function.

Influence functions encounter a challenge in direct application to deep models, primarily due to the non-convex nature of the loss function and the considerable size of model parameters. This obstacle not only renders the calculation of the inverse of the Hessian matrix costly but also leads to its non-existence. Various attempts, including matrix decomposition methods [10, 13, 3], have been undertaken to expedite and approximate the inversion of the Hessian matrix, aiming to render influence functions viable for deep models. In this paper, we revisit a particular naive yet aggressive approximation method TracIn [16] by substituting the inverse of the Hessian matrix with an identity matrix, outlined as follows:

$$\mathcal{I}_{\text{IP}}^{\text{util}}(-z_i) = \nabla v^{\text{util}} \nabla_{\hat{\theta}} \ell(z_i; \hat{\theta}), \text{ and } \nabla v^{\text{util}} = \sum_{z_j \in V} \nabla_{\hat{\theta}} \ell(z_j; \hat{\theta})^T. \quad (2)$$

The above equation is a Hessian-free approximation, which in essence is the inner product of ∇v^{util} and the sample gradient $\nabla_{\hat{\theta}} \ell(z_i; \hat{\theta})$; therefore, we call this method *Inner Product (IP)* in our paper. In the original paper [16], the authors employ gradient tracing to measure the sample influence, and explain its rationality from calculus; in the following, we link the IP to influence functions and provide our insights of IP on why such a naive approximation works well in practice.

Let $\nabla v^{\text{util}} = \sum_{z_j \in V} \nabla_{\hat{\theta}} \ell(z_j; \hat{\theta})^T$, then the influence functions in Eq. (1) and (2) can be reformulated as $\nabla v^{\text{util}} \mathbf{H}_{\hat{\theta}}^{-1} \nabla_{\hat{\theta}} \ell(z_i; \hat{\theta})$ and $\nabla v^{\text{util}} \nabla_{\hat{\theta}} \ell(z_i; \hat{\theta})$. It is worth noting that given the well-trained model parameters $\hat{\theta}$, ∇v^{util} and $\mathbf{H}_{\hat{\theta}}^{-1}$ remain constant. We can visualize the direction of $\nabla v^{\text{util}} \mathbf{H}_{\hat{\theta}}^{-1}$ and ∇v^{util} in Figure 1, with the influence scores roughly representing the angle between the sample gradient and $\nabla v^{\text{util}} \mathbf{H}_{\hat{\theta}}^{-1}$ or ∇v^{util} , where $\mathbf{H}_{\hat{\theta}}^{-1}$ induces a rotation of α between these two directions. Remarkably, although the influence scores calculated by Eq. (1) and (2) may differ, they exhibit order-consistency in several scenarios. For instance, if two samples z_i and $z_{i'}$ have gradients in Region II or IV, then $\mathcal{I}^{\text{util}}(-z_i) \geq \mathcal{I}^{\text{util}}(-z_{i'})$ implies $\mathcal{I}_{\text{IP}}^{\text{util}}(-z_i) \geq \mathcal{I}_{\text{IP}}^{\text{util}}(-z_{i'})$. However, this order-consistency does not hold in Regions I and III. Fortunately, the samples in these regions are jointly recognized by $\mathcal{I}^{\text{util}}$ and $\mathcal{I}_{\text{IP}}^{\text{util}}$ as beneficial or detrimental, which has little practical difference. A complete analysis can be found in Appendix A.

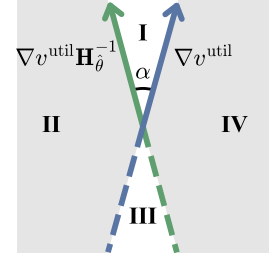


Figure 1: Visualization of the directions $\nabla v^{\text{util}} \mathbf{H}_{\hat{\theta}}^{-1}$ and ∇v^{util} .

In general, IP emerges as a straightforward, efficient, and remarkably effective alternative to influence functions, particularly in convex settings. However, in non-convex scenarios, approximations of the inverse Hessian matrix may introduce significant errors, rendering $\nabla v^{\text{util}} \mathbf{H}_{\hat{\theta}}^{-1}$ ineffective, even incorrect. We substantiate this observation empirically in Section 4. Conversely, while ∇v^{util} in IP may not precisely align with the optimal direction for enhancing model performance, it remains a reliable indicator for distinguishing between detrimental and beneficial samples, even for non-convex models. Intuitively, if a sample gradient aligns with the gradient from the validation set, it suggests that incorporating this sample contributes to enhancing the model's utility. Similarly, the negative impact of a single sample on prediction can also be mitigated by considering its gradient.

Extension. Beyond measuring the sample influence on model utility, we extend IP to assess the sample influence on fairness and robustness by modifying the impact function f .

Specifically, we can instantiate the impact function f by group fairness [43], such as demographic parity (DP) to measure influence on fairness [29]. Consider a binary sensitive attribute defined as $g \in \{0, 1\}$ and let \hat{y} denote the

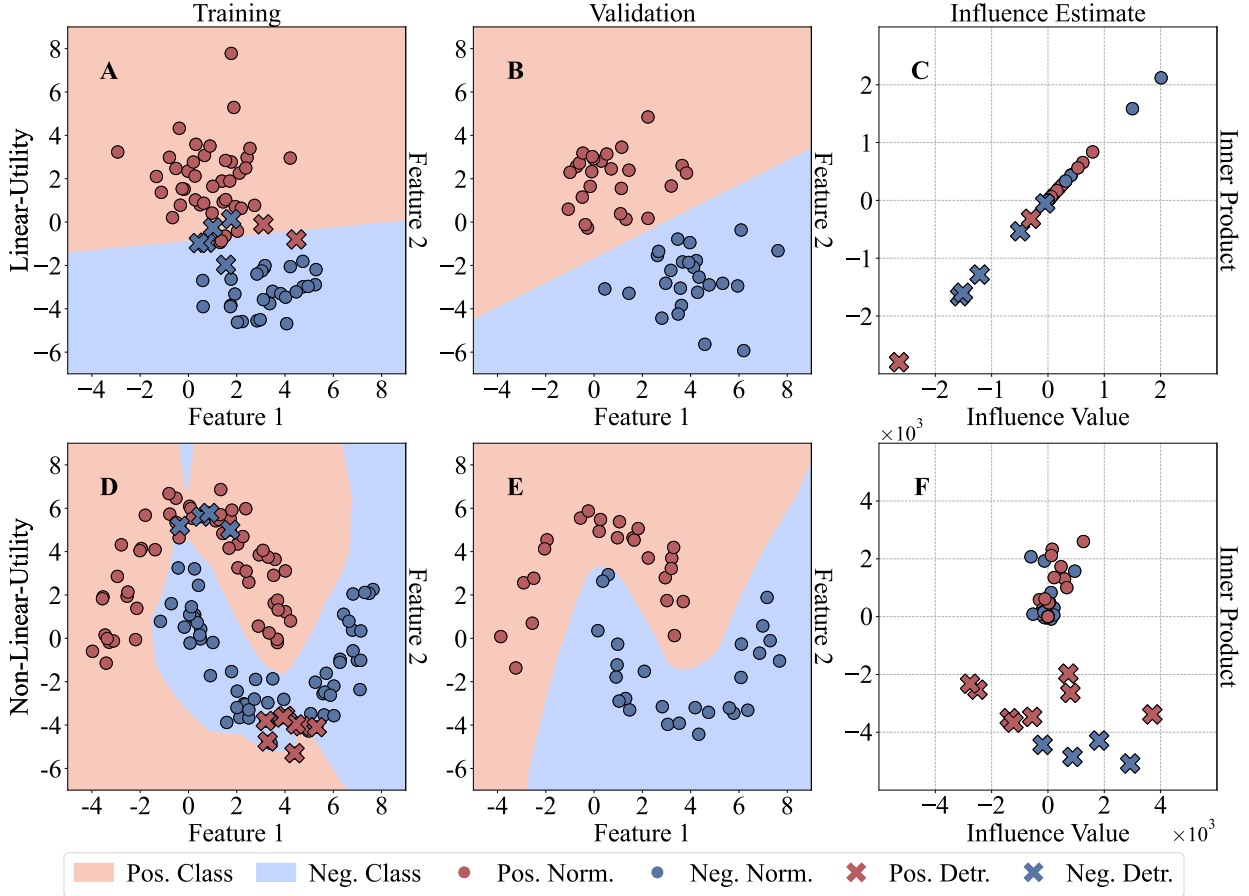


Figure 2: Illustrating our inner product approach on two synthetic datasets and convex/non-convex models. **A-C** illustrate a 2D linearly separable synthetic dataset with a subset of detrimental samples bearing incorrect labels, trained using a Logistic Regression model for binary classification, and **D-F** demonstrate the same analysis on a non-linear synthetic half-moon dataset with mislabeled samples, trained using a Multilayer Perceptron neural network. Specifically, **A** and **D** depict training sets with class labels 0 (red) and 1 (blue), where detrimental samples are marked with \times and regular samples with \circ . **B** and **E** show test sets utilized to assess model performance under convex and non-convex conditions. **C** and **F** present the calculated influence scores and inner product scores derived by Eq. (1) and (2), respectively. In the linear dataset with the convex model, there is a clear correlation between influence scores and inner product scores, the detrimental samples have both negative influence scores and inner product scores. However, in the non-linear dataset with the non-convex model, the influence scores of detrimental samples appear intermixed; fortunately, the detrimental samples are effectively isolated from inliers through inner product scores.

predicted class probabilities. The fairness metric DP is defined as: $f^{\text{DP-fair}}(\hat{\theta}, V) = |\mathbb{E}_V[\hat{y}|g=1] - \mathbb{E}_V[\hat{y}|g=0]|$. Within the above IP framework, we can calculate the training sample influence on fairness as follows:

$$\mathcal{I}_{\text{IP}}^{\text{DP-fair}}(-z_i) = \nabla v^{\text{fair}} \nabla_{\hat{\theta}} \ell(z_i; \hat{\theta}), \text{ and } \nabla v^{\text{fair}} = \nabla_{\hat{\theta}} f^{\text{DP-fair}}(\hat{\theta}, V)_{\hat{\theta}}^{\top}. \quad (3)$$

Similarly, we can also measure the sample influence on adversarial robustness within the IP framework. To achieve this, we follow [2] and consider a white-box adversary [44] specific to linear models, which can be easily extended to other models and settings. To craft an adversarial sample, we take each sample $z_j = (x_j, y_j)$ in the validation set V and only perturb $x'_j = x_j - \gamma \frac{\hat{\theta}^{\top} x_j + b}{\hat{\theta}^{\top} \hat{\theta}} \hat{\theta}$ and keep y_j unchanged, where $\hat{\theta} \in \mathbb{R}^d$ are the linear model coefficients, $b \in \mathbb{R}$ is the intercept, and $\gamma > 1$ controls the amount of perturbation added. In this manner, we can obtain an adversarial validation set V' which consists of $z'_j = (x'_j, y_j)$ for each sample z_j of V . Now, we can compute adversarial robustness influence for each training sample as follows:

$$\mathcal{I}_{\text{IP}}^{\text{robust}}(-z_i) = \nabla v^{\text{robust}} \nabla_{\hat{\theta}} \ell(z_i; \hat{\theta}), \text{ and } \nabla v^{\text{robust}} = \sum_{z'_j \in V'} \nabla_{\hat{\theta}} \ell(z'_j; \hat{\theta})^{\top}. \quad (4)$$

Enhancement: The simplicity inherent in the IP framework offers opportunities to enhance the generalization of influence functions. In convex cases, the model parameter $\hat{\theta}$ is both optimal and unique. However, in non-convex

Table 1: Accuracy results of influence function-based methods on the *CIFAR10N*, *CIFAR-100N* and *Animal-10N* datasets with 5% identified detrimental samples removed

Methods / Datasets	<i>CIFAR-10N-a</i>	<i>CIFAR-10N-r</i>	<i>CIFAR-10N-w</i>	<i>CIFAR-100N</i>	<i>Animal-10N</i>	Avg.
Cross Entropy	91.62	90.25	85.66	56.41	80.54	80.90
TracIn [16]	91.91 ± 0.25	90.73 ± 0.35	85.86 ± 0.18	58.18 ± 0.25	82.00 ± 0.04	81.74
LiSSA [10]	92.13 ± 0.29	90.98 ± 0.16	85.97 ± 0.47	59.24 ± 0.39	81.93 ± 0.14	82.05
EKFAC [13]	91.76 ± 0.23	90.47 ± 0.10	83.25 ± 0.38	59.91 ± 0.90	80.89 ± 0.54	81.26
DataInf [3]	91.88 ± 0.39	90.79 ± 0.21	86.22 ± 0.13	58.40 ± 0.22	81.60 ± 0.23	81.78
Self-TracIn [18]	92.03 ± 0.09	90.43 ± 0.24	86.00 ± 0.18	61.99 ± 0.29	81.82 ± 0.34	82.45
Self-LiSSA [17]	91.91 ± 0.17	90.66 ± 0.35	85.73 ± 0.41	61.56 ± 0.56	81.23 ± 0.24	82.22
IP Ensemble (Ours)	92.26 ± 0.19	91.28 ± 0.29	86.50 ± 0.35	62.25 ± 0.54	82.35 ± 0.55	82.93

scenarios, the presence of local minima introduces instability and non-uniqueness into the solution. Typically, ensemble strategies are employed to bolster model generalization. Yet, while employing different models can enhance performance, it also escalates the costs associated with model training and complicates the calculation of influence functions. This arises from the variability in model parameters, necessitating multiple computations of the inverse of each individual Hessian matrix. The introduction of Hessian-free IP circumvents this issue, eliminating the need for costly calculations of Hessian matrices and their inverses. Drawing inspiration from dropout mechanisms, diverse models can be swiftly generated without necessitating model retraining. By computing sample gradients from various models, we propose IP Ensemble that amalgamates IP scores from distinct models. Experiments detailed in Section 5 illustrate the superior performance of the inner product ensemble over other influence function-based methods.

4 Correctness Verification on Synthetic Data

Here we verify the correctness of our Inner Product (IP) as an influence score surrogate on two synthetic datasets with convex/non-convex models. First, we use Logistic Regression on a linear dataset to demonstrate the effectiveness of IP in a convex optimization scenario. Second, we use a Multi Layer Perceptron on a half-moon dataset to validate the performance of IP in a non-convex optimization scenario.² In Figure 2, **A** and **B** illustrate the training and test sets of a linearly separable dataset, consisting of 150 and 100 samples, respectively. Notably, the training set contains 10 manually generated noisy samples with incorrect labels. Similarly, **D-F** illustrate a non-linear separable half-moons dataset, consisting of 200 training samples including 20 noisy samples with incorrect labels, and 100 test samples. **C** and **F** display the influence score and inner product score for each training sample, calculated according to Eq. (1) and (2), respectively. Beyond model utility, we also verify the correctness of IP on model fairness and robustness in Appendix C.1.

In the linear case depicted in Figure 2**C**, the inner product score serves as a reliable surrogate to distinguish detrimental samples from beneficial ones. It exhibits an almost perfect correlation and order-consistency with the influence score. Specifically, detrimental samples yield negative scores for both inner product and influence, while other samples typically show positive or nearly zero values. Figure 3 illustrates the relationship between directions among ∇v^{util} , $\nabla v^{\text{util}} \mathbf{H}_{\hat{\theta}}^{-1}$, and the gradients of detrimental samples. It is worth noting that the angle between $\nabla v^{\text{util}} \mathbf{H}_{\hat{\theta}}^{-1}$ and ∇v^{util} is only 0.66° , indicating that the identity matrix is a simple and effective surrogate of $\mathbf{H}_{\hat{\theta}}^{-1}$ in the linear case.

However, the limitations of influence scores become apparent in the context of non-convex models, as illustrated in Figure 2**F**. Here, the influence scores of detrimental samples are intermingled with those of normal ones, where $\nabla v^{\text{util}} \mathbf{H}_{\hat{\theta}}^{-1}$ is not the optimal direction due to the inaccuracies in approximating the Hessian matrix. Fortunately, the IP score effectively isolates detrimental samples from inliers. Even for this non-linear dataset, ∇v^{util} remains a useful indicator for discerning detrimental samples from beneficial ones, as all detrimental samples exhibit obtuse angles with ∇v^{util} .

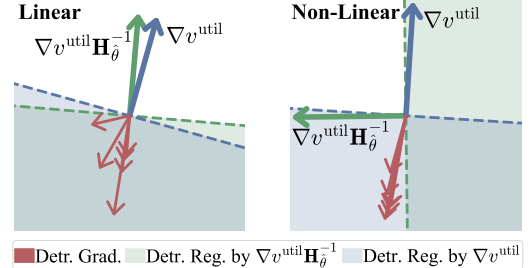


Figure 3: Directions of gradients of the validation set and detrimental samples of the datasets in Figure 2. In the linear case, α is 0.66° , and we draw a larger angle for better visualization. For the non-linear case, we use the dimension reduction [45] for visualization, and α is 94.36° .

²The detailed characteristics of datasets and models used in this paper can be found in Appendix B.

5 Noisy Label Correction for Vision Datasets

In this section, we demonstrate the effectiveness of our IP Ensemble in identifying samples with noisy labels on vision datasets. Specifically, we choose three benchmark datasets *CIFAR-10N* [46], *CIFAR-100N* [46], and *Animal-10N* datasets [47] in the noisy label learning area, all of which are derivatives of the original *CIFAR-10* [48], *CIFAR-100* [48], and *Animal-10* [49], but incorporate label inaccuracies from crowd-sourced annotation. *CIFAR-10N* encompasses three distinct noise settings: aggregate, random, and worst, denoted as “-a”, “-r”, and “-w”, respectively. In the aggregate setting, labels are derived via majority voting among three annotators, with ties being resolved randomly. The random setting adopts the label provided by the first annotator, while the worst setting selects the label from the least reliable annotator.

For the competitive methods, we choose the following influence function-based methods. TracIn [16] replaces the Hessian matrix with the identity matrix; LiSSA [10] and EKFAC [13] employ implicit Hessian-vector products and Kronecker-Factored curvature to efficiently approximate the inverse of the Hessian matrix; DataInf [3] swaps the order of the matrix multiple for obtaining a closed-form expression; Self-TracIn [18] and Self-LiSSA [17] are the self-expression versions of TracIn and LiSSA, where ∇v^{util} is replaced with $\nabla_{\hat{\theta}}\ell(z_i; \hat{\theta})$, leading their self-influence to $\ell(z_i; \hat{\theta})^\top \nabla_{\hat{\theta}}\ell(z_i; \hat{\theta})$ or $\ell(z_i; \hat{\theta})^\top \mathbf{H}_{\hat{\theta}}^{-1} \nabla_{\hat{\theta}}\ell(z_i; \hat{\theta})$. Our IP closely resembles TracIn, with the additional application of dropout with $\mathcal{U}(0, 0.01)$ on the model parameters. Furthermore, our IP Ensemble constitutes an ensemble version of IP with an ensemble size of 5.

To reduce randomness, we train a ResNet-34 network [50] once on each dataset to establish a baseline model. Subsequently, based on the same model, we employ the aforementioned influence function-based methods to identify 5% of detrimental samples. Following this, we conduct five retraining iterations of the ResNet-34 network, each time removing the identified detrimental samples from the training set. We report the average accuracy and standard deviation of the above influence function-based methods across these five retraining iterations in Table 1. In general, these influence function-based methods are effective in identifying detrimental samples. Upon retraining the ResNet-34 model without these identified samples, nearly every result obtained by these methods outperforms the vanilla ResNet-34 trained on the entire dataset, except for EKFAC on *CIFAR-10N-w*. Notably, our IP Ensemble consistently outperform other baseline methods across various noise conditions and datasets. Particularly noteworthy is the performance of our IP Ensemble in the most challenging scenario, *CIFAR-100N*, achieving the highest recorded accuracy of 62.25% on the test set, surpassing the vanilla cross-entropy accuracy of 56.41%. Additionally, compared to TracIn, the non-ensemble version of IP, IP Ensemble delivers further performance gains, highlighting the benefits of the ensemble strategy for enhancing model generalization. Moreover, the average accuracy of the IP Ensemble on the test set reaches its peak at 82.93%, surpassing both the vanilla cross-entropy performance of 80.90% and the second-best accuracy of Self-TracIn at 82.45%. More experimental results and analysis on different percentage of removed samples, parameter analysis on different dropout rates and different ensemble size can be found in Appendix C.2 and C.3, respectively.

In addition to the algorithmic performance mentioned above, we also present the running times of various influence function-based methods for identifying detrimental samples. Despite some baselines having linear time complexity, there is significant divergence in their real execution times. Given that TracIn and our IP Ensemble exhibit exceptional speed and similar execution times, we consider them as the baseline and compute the speed improvement factors over other baseline methods, as depicted in Figure 4. With the exception of Self-TracIn, our IP runs over 100 times faster than LiSSA, EKFAC, DataInf, and Self-LiSSA. Notably, on *Animal-10N*, IP is over 800 times faster than EKFAC. It’s worth noting that Self-TracIn and Self-LiSSA are slower than their standard versions due to the fixed ∇v^{util} when calculating the influence of each sample. The simplicity and efficiency of IP make it a promising tool for analyzing sample influence on deep models. The time complexities and execution time of these methods can be found in Appendix C.4.

6 Data Curation Towards Fine-Tuning of Fairer NLP Models

In this section, we further demonstrate the efficacy of our IP method in gauging the impact of individual samples on fairness within the realm of curating suitable data samples for fine-tuning Natural Language Processing (NLP) models. Beyond mere utility, fairness has emerged as an indispensable attribute for machine learning models to mitigate inadvertent discrimination.

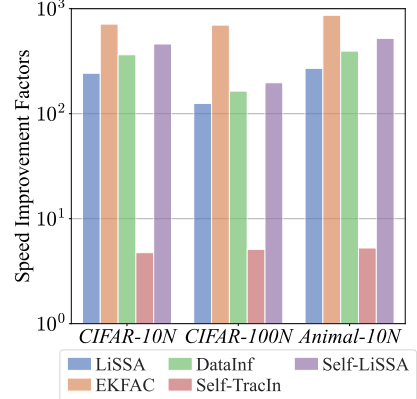


Figure 4: Speed improvement factors of IP over other baseline methods.

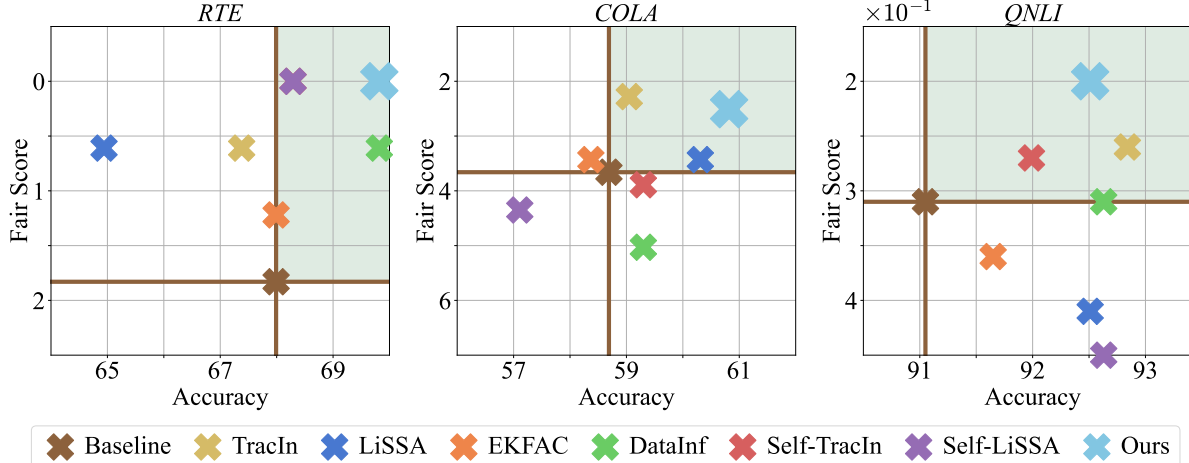


Figure 5: Accuracy and fair score of different influence function-based methods on fine-tuning *RTE*, *COLA*, and *QNLI* datasets. The X-axis denotes accuracy, and the Y-axis for fair score is inverted. The brown crossing denotes the performance of using all the samples for fine-tuning the RoBERTa model as the baseline model. Building upon this, we plot a horizontal and a vertical line in each figure and divide the space by fairness and utility results into four regions. The green area in the top right corner signifies a model that is both fairer and more accurate compared to the baseline model.

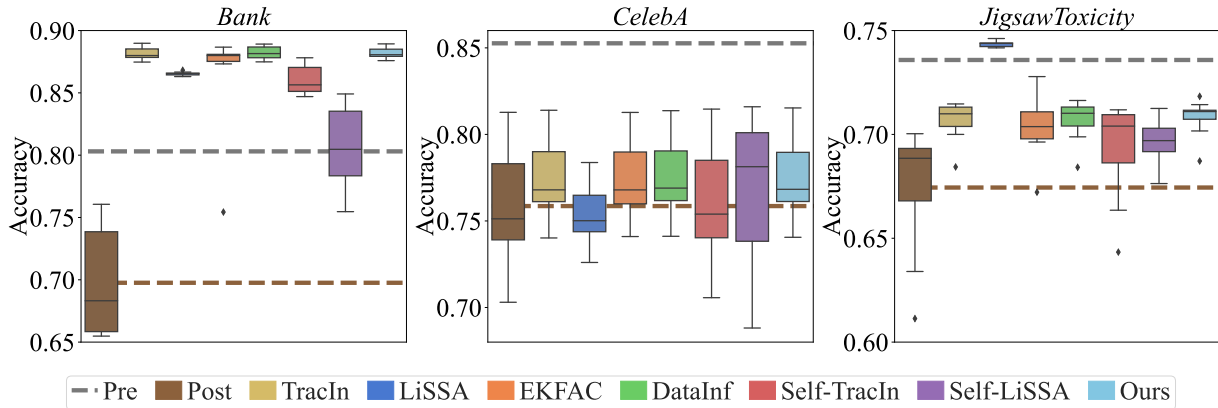
In this experiment, we employ three datasets—*RTE*, *COLA*, and *QNLI*—from the GLUE repository [51] to fine-tune the widely-used language model pre-training model RoBERTa [52]. Our focus is on group fairness, necessitating that machine learning models treat samples within various predefined subgroups comparably. To assess fairness, we adopt the methodology outlined in [53], which involves perturbing the demographic information within each sample and scrutinizing whether the model yields identical predictions for the original sample x and its corresponding perturbed counterpart \tilde{x} . This evaluation metric "fair score" is defined as $|\mathcal{C}(x) - \mathcal{C}(\tilde{x})|$ over all the samples in the test set, normalized by the size of the test set, where $\mathcal{C}(\cdot)$ is the model predictor. It is worth to note that the fair score is a negative metric, indicating that smaller values are preferable.

Utility and fairness serve as distinct perspectives for evaluating the performance of a model. While a constant predictor that consistently outputs the same prediction, regardless of input, can achieve perfect fairness, it lacks practical flexibility. Thus, in our fine-tuning experiments, we consider both utility and fairness. Employing the same influence function-based methods and our IP Ensemble as in the previous section, we conduct a comparative analysis. For each method, we calculate the influence on both utility and fairness within the fine-tuning set. We then identify and remove the 5% most detrimental samples in terms of utility and fairness before fine-tuning the RoBERTa model to optimize performance across both accuracy and fairness metrics.

The results of this experiment are presented in Figure 5, where the Y-axis for fairness is inverted. The brown crossing denotes the performance of using all the samples for model fine-tuning as the base model. Building upon this, we plot a horizontal and a vertical line in each figure and divide the space by fairness and utility results into four regions. The green area in the top right corner signifies a model that is both fairer and more accurate compared to the baseline model. Results within this green region can be considered Pareto improvements, enhancing both utility and fairness simultaneously. It is evident most results are located in the green area, indicating the existence of detrimental samples, and not all the samples are helpful to the model performance. This also implies that influence function methods are effective to identifying the detrimental samples, even for non-convex deep models. However, it is important to note that some competitive methods yield a trade-off or even Pareto deterioration. For instance, LiSSA demonstrates a better fair score but worse accuracy compared to the base model on *RTE*; conversely, it exhibits better accuracy but worse fairness on *QNLI*. EKFAC shows similar performance on *COLA* and *QNLI*. Self-LiSSA demonstrates Pareto deterioration on *COLA*. We hypothesize that the approximation of the inverse of the Hessian matrix may suffer from large errors, leading to heavily divergent influence estimations from the true values. Our IP Ensemble consistently achieves Pareto improvements across all three datasets, often yielding the best results compared to other influence function-based methods.

Table 2: Defense performance of various influence function-based methods under the relabeling and reweighting strategies on *Bank*, *CelebA*, and *JigsawToxicity* datasets

Defense Strategy	Relabeling				Reweighting			
	<i>Bank</i>	<i>CelebA</i>	<i>JigsawToxicity</i>	Avg	<i>Bank</i>	<i>CelebA</i>	<i>JigsawToxicity</i>	Avg
Pre	80.31	85.26	73.58	79.72	80.31	85.26	73.58	79.72
Post	70.79 ± 3.71	75.33 ± 3.04	66.18 ± 3.52	70.77	70.79 ± 3.71	75.33 ± 3.04	66.18 ± 3.52	70.77
TracIn [16]	87.44 ± 0.26	77.28 ± 1.87	70.43 ± 0.87	78.38	86.17 ± 2.04	75.10 ± 1.71	70.82 ± 0.36	77.36
LiSSA [10]	86.07 ± 0.39	68.68 ± 1.39	73.30 ± 2.96	76.02	78.69 ± 3.56	73.23 ± 3.70	70.13 ± 1.00	74.02
EKFAC [13]	87.38 ± 0.89	77.36 ± 1.94	70.04 ± 0.96	78.26	83.50 ± 5.90	75.11 ± 1.73	70.05 ± 0.76	76.22
DataInf [3]	87.46 ± 2.44	77.36 ± 1.85	70.39 ± 0.84	78.40	85.99 ± 2.49	74.74 ± 1.68	70.82 ± 0.35	77.18
Self-TracIn [18]	86.12 ± 1.10	75.58 ± 2.97	68.31 ± 2.73	76.67	85.22 ± 1.72	73.12 ± 3.71	71.37 ± 1.81	76.57
Self-LiSSA [17]	78.97 ± 3.40	75.55 ± 2.99	69.18 ± 1.76	74.57	85.16 ± 1.74	73.17 ± 3.72	71.41 ± 1.86	76.58
IP Ensemble (Ours)	87.45 ± 0.32	77.30 ± 1.89	70.51 ± 1.00	78.42	86.44 ± 2.58	75.10 ± 1.73	70.67 ± 0.27	77.40

Figure 6: Performance variations across various influence function-based methods over 10 distinct attacks on *Bank*, *CelebA*, and *JigsawToxicity*. The dashed gray line presents the pre-attack performance, while the brown line denotes the average accuracy of post-attack over 10 runs.

7 Defense Against Adaptive Evasion Adversaries

In this section, we demonstrate how the influence-based approach can effectively fortify defenses against an adaptive adversary [54, 55] that performs evasion attacks on the learning model. In this scenario, the attacker randomly selects a subset of test samples to launch the evasion attack. We defend by proactively trimming the training set by a predetermined amount, although we lack specific knowledge about which samples are adversarial during inference.

In this experiment, we utilize a Logistic Regression model with three datasets: *Bank* [56], *CelebA* [57], and *JigsawToxicity* [58]. Following the protocol in Section 3, we consider a white-box adversary [44] to craft adversarial samples. For each sample (x_j, y_j) in the validation set \mathcal{V} , we perturb it by changing the feature $x'_j = x_j - \gamma \frac{\hat{\theta}^\top x_j + b}{\hat{\theta}^\top \hat{\theta}} \hat{\theta}$ and keeping y_j unchanged. The attacker perturbs between 5% and 25% of the test set samples at random. By quantifying the impact of samples on model robustness, we trim 5% detrimental samples in the training set through influence functions. The boxplot depicted in Figure 6 demonstrates the performance variations across various influence function-based methods over 10 distinct attacks. In general, influence function-based methods are highly effective against adaptive evasion attackers, showcasing superior resilience particularly post-attack, notably evident in scenarios involving *Bank* and *JigsawToxicity*. Among these influence function-based methods, our IP Ensemble demonstrates competitive efficacy with the best or the second best on these three datasets.

In addition to the above removing strategy, we continue to explore relabeling and reweighting strategies to tackle detrimental samples. The relabeling strategy [20] changes the identified detrimental samples from their original classes into another class, since the datasets we used here are binary classes, we directly flip their labels. The reweighting strategy [18] takes the influence score of each sample as the exponential weight with a softmax normalization, and then trains a model with weighted gradient. We report the defense performance of various influence function-based methods and our IP Ensemble under the relabeling and reweighting strategies in Table 2.

Under the relabeling strategy, DataInf achieves the best results on *Bank* and *CelebA* with 87.46% and 77.36% accuracy, respectively. However, LiSSA is not stable as other methods on *CelebA* with only 68.68%, which is even worse than the performance of post attack. Our IP ensemble method continues to achieve competitive performance, with accuracy scores of 87.45%, 77.30%, and 70.51% on three datasets with the second-best performance among all influence functions-based methods. For the reweighting strategy, the influence function-based methods are still effective on *Bank* and *JigsawToxicity*, which outperform the post-attack by a large margin, but achieve similar performance with post attack on *CelebA*. Notably, when considering the average accuracy of both the relabeling and reweighting strategies, our IP Ensemble method performs the best.

8 Conclusion

In this paper, we revisited, extended, and enhanced the TracIn method into the Inner Product (IP) formulation. By proving the exhibition of order-consistency in several scenarios between IP and Influence function, we demonstrated how substituting the inverse of the Hessian matrix with an identity matrix offers a practical and computationally efficient solution to estimating sample influence. Based on that, we extended our IP to measure the sample influence on fairness and robustness. Continually, we enhanced the generalization of IP by introducing an ensemble strategy. We verified the correctness of IP on synthetic datasets and extensive evaluations on noisy label detection, data curation for fair NLP model fine-tuning, and defense against adaptive adversarial attacks. Overall, our IP Ensemble highlighted the potential of simple, yet powerful, approximations in influence estimation. By broadening the scope of TracIn and improving its robustness and fairness applications, we provided valuable tools for data-centric learning and model interpretation, offering practical solutions for contemporary challenges in deep learning.

References

- [1] Luis Oala, Manil Maskey, Lilith Bat-Leah, Alicia Parrish, Nezihe Merve Gürel, Tzu-Sheng Kuo, Yang Liu, Rotem Dror, Danilo Brajovic, Xiaozhe Yao, et al. Dmlr: Data-centric machine learning research—past, present and future. *arXiv preprint arXiv:2311.13028*, 2023.
- [2] Anshuman Chhabra, Peizhao Li, Prasant Mohapatra, and Hongfu Liu. What data benefits my classifier? enhancing model performance and interpretability through influence-based data selection. In *International Conference on Learning Representations*, 2024.
- [3] Yongchan Kwon, Eric Wu, Kevin Wu, and James Zou. Datainf: Efficiently estimating data influence in lora-tuned llms and diffusion models. *arXiv preprint arXiv:2310.00902*, 2023.
- [4] Zayd Hammoudeh and Daniel Lowd. Training data influence analysis and estimation: A survey. *arXiv preprint arXiv:2212.04612*, 2022.
- [5] R Dennis Cook and Sanford Weisberg. *Residuals and influence in regression*. New York: Chapman and Hall, 1982.
- [6] Amirata Ghorbani and James Zou. Data shapley: Equitable valuation of data for machine learning. In *International Conference on Machine Learning*, 2019.
- [7] Ruoxi Jia, David Dao, Boxin Wang, Frances Ann Hubis, Nick Hynes, Nezihe Merve Gürel, Bo Li, Ce Zhang, Dawn Song, and Costas J Spanos. Towards efficient data valuation based on the Shapley value. In *International Conference on Artificial Intelligence and Statistics*, 2019.
- [8] Yongchan Kwon and James Zou. Beta Shapley: a Unified and Noise-reduced Data Valuation Framework for Machine Learning. In *International Conference on Artificial Intelligence and Statistics*, 2022.
- [9] Ruoxi Jia, David Dao, Boxin Wang, Frances Ann Hubis, Nezihe Merve Gurel, Bo Li, Ce Zhang, Costas Spanos, and Dawn Song. Efficient task specific data valuation for nearest neighbor algorithms. In *International Conference on Very Large Data Bases Endowment*, 2018.
- [10] Pang Wei Koh and Percy Liang. Understanding black-box predictions via influence functions. In *International Conference on Machine Learning*, 2017.
- [11] Naman Agarwal, Brian Bullins, and Elad Hazan. Second-order stochastic optimization for machine learning in linear time. *Journal of Machine Learning Research*, 2017.
- [12] Juhan Bae, Nathan Ng, Alston Lo, Marzyeh Ghassemi, and Roger B Grosse. If influence functions are the answer, then what is the question? *Advances in Neural Information Processing Systems*, 2022.
- [13] Roger Grosse, Juhan Bae, Cem Anil, Nelson Elhage, Alex Tamkin, Amirhossein Tajdini, Benoit Steiner, Dustin Li, Esin Durmus, Ethan Perez, et al. Studying large language model generalization with influence functions. *arXiv preprint arXiv:2308.03296*, 2023.

- [14] Samyadeep Basu, Philip Pope, and Soheil Feizi. Influence functions in deep learning are fragile. *arXiv preprint arXiv:2006.14651*, 2020.
- [15] Jacob R Epifano, Ravi P Ramachandran, Aaron J Masino, and Ghulam Rasool. Revisiting the fragility of influence functions. *Neural Networks*, 162:581–588, 2023.
- [16] Garima Pruthi, Frederick Liu, Satyen Kale, and Mukund Sundararajan. Estimating training data influence by tracing gradient descent. *Advances in Neural Information Processing Systems*, 2020.
- [17] Irina Bejan, Artem Sokolov, and Katja Filippova. Make every example count: On the stability and utility of self-influence for learning from noisy nlp datasets. *arXiv preprint arXiv:2302.13959*, 2023.
- [18] Megh Thakkar, Tolga Bolukbasi, Sriram Ganapathy, Shikhar Vashisht, Sarath Chandar, and Partha Talukdar. Self-influence guided data reweighting for language model pre-training. *arXiv preprint arXiv:2311.00913*, 2023.
- [19] Zayd Hammoudeh and Daniel Lowd. Training data influence analysis and estimation: A survey. *Machine Learning*, pages 1–53, 2024.
- [20] Shuming Kong, Yanyan Shen, and Linpeng Huang. Resolving training biases via influence-based data relabeling. In *International Conference on Learning Representations*, 2021.
- [21] Zifeng Wang, Hong Zhu, Zhenhua Dong, Xiuqiang He, and Shao-Lun Huang. Less is better: Unweighted data subsampling via influence function. In *AAAI Conference on Artificial Intelligence*, 2020.
- [22] Daniel Ting and Eric Brochu. Optimal subsampling with influence functions. *Advances in Neural Information Processing Systems*, 2018.
- [23] Boris Sharchilev, Yury Ustinovskiy, Pavel Serdyukov, and Maarten Rijke. Finding influential training samples for gradient boosted decision trees. In *International Conference on Machine Learning*, 2018.
- [24] Mengzhou Xia, Sadhika Malladi, Suchin Gururangan, Sanjeev Arora, and Danqi Chen. Less: Selecting influential data for targeted instruction tuning. *arXiv preprint arXiv:2402.04333*, 2024.
- [25] Seulki Park, Jongin Lim, Younghan Jeon, and Jin Young Choi. Influence-balanced loss for imbalanced visual classification. In *IEEE/CVF International Conference on Computer Vision*, 2021.
- [26] Yuyuan Li, Chaochao Chen, Xiaolin Zheng, Yizhao Zhang, Biao Gong, Jun Wang, and Linxun Chen. Selective and collaborative influence function for efficient recommendation unlearning. *Expert Systems with Applications*, 2023.
- [27] Yang Zhang, Zhiyu Hu, Yimeng Bai, Fuli Feng, Jiancan Wu, Qifan Wang, and Xiangnan He. Recommendation unlearning via influence function. *arXiv preprint arXiv:2307.02147*, 2023.
- [28] Zhuoming Liu, Hao Ding, Huaping Zhong, Weijia Li, Jifeng Dai, and Conghui He. Influence selection for active learning. In *IEEE/CVF International Conference on Computer Vision*, 2021.
- [29] Peizhao Li and Hongfu Liu. Achieving fairness at no utility cost via data reweighing with influence. In *International Conference on Machine Learning*, 2022.
- [30] Jialu Wang, Xin Eric Wang, and Yang Liu. Understanding instance-level impact of fairness constraints. In *International Conference on Machine Learning*, 2022.
- [31] Haonan Wang, Ziwei Wu, and Jingrui He. Fairif: Boosting fairness in deep learning via influence functions with validation set sensitive attributes. In *International Conference on Web Search and Data Mining*, 2024.
- [32] Gilad Cohen, Guillermo Sapiro, and Raja Giryes. Detecting adversarial samples using influence functions and nearest neighbors. In *IEEE/CVF Conference on Computer Vision and Pattern Recognition*, 2020.
- [33] Zizhang Chen, Peizhao Li, Hongfu Liu, and Pengyu Hong. Characterizing the influence of graph elements. In *International Conference on Learning Representations*, 2023.
- [34] Jiancan Wu, Yi Yang, Yuchun Qian, Yongduo Sui, Xiang Wang, and Xiangnan He. Gif: A general graph unlearning strategy via influence function. In *ACM Web Conference*, 2023.
- [35] Jie Xu, Zihan Wu, Cong Wang, and Xiaohua Jia. Machine unlearning: Solutions and challenges. *IEEE Transactions on Emerging Topics in Computational Intelligence*, 2024.
- [36] Ayush K Tarun, Vikram S Chundawat, Murari Mandal, and Mohan Kankanhalli. Fast yet effective machine unlearning. *IEEE Transactions on Neural Networks and Learning Systems*, 2023.
- [37] Haotian Ye, Chuanlong Xie, Yue Liu, and Zhenguo Li. Out-of-distribution generalization analysis via influence function. *arXiv preprint arXiv:2101.08521*, 2021.
- [38] Alycia N Carey, Minh-Hao Van, and Xintao Wu. Evaluating the impact of local differential privacy on utility loss via influence functions. *arXiv preprint arXiv:2309.08678*, 2023.

- [39] Jieyu Zhang, Haonan Wang, Cheng-Yu Hsieh, and Alexander J Ratner. Understanding programmatic weak supervision via source-aware influence function. *Advances in Neural Information Processing Systems*, 2022.
- [40] Pang Wei W Koh, Kai-Siang Ang, Hubert Teo, and Percy S Liang. On the accuracy of influence functions for measuring group effects. *Advances in Neural Information Processing Systems*, 2019.
- [41] Hyeonsu Lyu, Jonggyu Jang, Sehyun Ryu, and Hyun Jong Yang. Deeper understanding of black-box predictions via generalized influence functions. *arXiv preprint arXiv:2312.05586*, 2023.
- [42] Hongge Chen, Si Si, Yang Li, Ciprian Chelba, Sanjiv Kumar, Duane Boning, and Cho-Jui Hsieh. Multi-stage influence function. *Advances in Neural Information Processing Systems*, 2020.
- [43] Cynthia Dwork, Moritz Hardt, Toniann Pitassi, Omer Reingold, and Richard Zemel. Fairness through awareness. In *Innovations in Theoretical Computer Science Conference*, 2012.
- [44] István Megyeri, István Hegedűs, and Márk Jelasity. Adversarial robustness of linear models: regularization and dimensionality. In *European Symposium on Artificial Neural Networks, Computational Intelligence and Machine Learning*, 2019.
- [45] Ella Bingham and Heikki Mannila. Random projection in dimensionality reduction: applications to image and text data. In *ACM SIGKDD International Conference on Knowledge Discovery and Data Mining*, 2001.
- [46] Jiaheng Wei, Zhaowei Zhu, Hao Cheng, Tongliang Liu, Gang Niu, and Yang Liu. Learning with noisy labels revisited: A study using real-world human annotations. In *International Conference on Learning Representations*, 2022.
- [47] Jun Shu, Xiang Yuan, Deyu Meng, and Zongben Xu. Cmw-net: Learning a class-aware sample weighting mapping for robust deep learning. *IEEE Transactions on Pattern Analysis and Machine Intelligence*, 2023.
- [48] Alex Krizhevsky, Geoffrey Hinton, et al. Learning multiple layers of features from tiny images. 2009.
- [49] Zhanpeng Zhang, Ping Luo, Chen Change Loy, and Xiaoou Tang. Learning deep representation for face alignment with auxiliary attributes. *IEEE Transactions on Pattern Analysis and Machine Intelligence*, 2015.
- [50] Kaiming He, Xiangyu Zhang, Shaoqing Ren, and Jian Sun. Deep residual learning for image recognition. In *IEEE Conference on Computer Vision and Pattern Recognition*, 2016.
- [51] Alex Wang, Amanpreet Singh, Julian Michael, Felix Hill, Omer Levy, and Samuel R Bowman. Glue: A multi-task benchmark and analysis platform for natural language understanding. *arXiv preprint arXiv:1804.07461*, 2018.
- [52] Yinhan Liu, Myle Ott, Naman Goyal, Jingfei Du, Mandar Joshi, Danqi Chen, Omer Levy, Mike Lewis, Luke Zettlemoyer, and Veselin Stoyanov. Roberta: A robustly optimized bert pretraining approach. *arXiv preprint arXiv:1907.11692*, 2019.
- [53] Rebecca Qian, Candace Ross, Jude Fernandes, Eric Michael Smith, Douwe Kiela, and Adina Williams. Perturbation augmentation for fairer NLP. In *Conference on Empirical Methods in Natural Language Processing*, 2022.
- [54] Florian Tramer, Nicholas Carlini, Wieland Brendel, and Aleksander Madry. On adaptive attacks to adversarial example defenses. *Advances in Neural Information Processing Systems*, 2020.
- [55] Battista Biggio, Igino Corona, Davide Maiorca, Blaine Nelson, Nedim Šrndić, Pavel Laskov, Giorgio Giacinto, and Fabio Roli. Evasion attacks against machine learning at test time. In *European Conference on Machine Learning and Principles and Practice of Knowledge Discovery in Databases*, 2013.
- [56] Sérgio Moro, Paulo Cortez, and Paulo Rita. A data-driven approach to predict the success of bank telemarketing. *Decision Support Systems*, 2014.
- [57] Ziwei Liu, Ping Luo, Xiaogang Wang, and Xiaoou Tang. Large-scale Celebfaces attributes (CelebA) dataset. *Retrieved August*, 2018.
- [58] David Noever. Machine learning suites for online toxicity detection. *arXiv preprint arXiv:1810.01869*, 2018.
- [59] Avital Oliver, Augustus Odena, Colin A Raffel, Ekin Dogus Cubuk, and Ian Goodfellow. Realistic evaluation of deep semi-supervised learning algorithms. *Advances in Neural Information Processing Systems*, 2018.

Appendix

A Rationality of Inner Product

In Figure 1, we visualize the direction of $\nabla v^{\text{util}} \mathbf{H}_{\hat{\theta}}^{-1}$ and ∇v^{util} , with the influence scores roughly representing the angle between the sample gradient and $\nabla v^{\text{util}} \mathbf{H}_{\hat{\theta}}^{-1}$ or ∇v^{util} , where $\mathbf{H}_{\hat{\theta}}^{-1}$ induces a rotation of α between these two directions. For a complete analysis, we further split Region II and IV into Sub-Regions as shown in Figure 7 assuming $\alpha < 45^\circ$. Given gradients of two samples z_i and $z_{i'}$, we analyze all possible scenarios as follows.

- **(I, I).** For a case where both z_i and $z_{i'}$ have gradients in Region I, $\mathcal{I}^{\text{util}}(-z_i) \gtrless \mathcal{I}^{\text{util}}(-z_{i'})$ implies $\mathcal{I}_{\text{IP}}^{\text{util}}(-z_{i'}) \gtrless \mathcal{I}_{\text{IP}}^{\text{util}}(-z_i)$, which is the opposite of order-consistency. While these samples are jointly recognized by $\mathcal{I}^{\text{util}}$ and $\mathcal{I}_{\text{IP}}^{\text{util}}$ as detrimental, there is little practical difference.
- **(I, II).** For a case where z_i has gradients in Region I and $z_{i'}$ has gradients in Region II, the order-consistency partially holds, depending on which Sub-Region the gradients of $z_{i'}$ is in. For Sub-Region II^b and II^c , we have $\mathcal{I}^{\text{util}}(-z_i) > \mathcal{I}^{\text{util}}(-z_{i'})$ and $\mathcal{I}_{\text{IP}}^{\text{util}}(-z_i) > \mathcal{I}_{\text{IP}}^{\text{util}}(-z_{i'})$, and the order-consistency holds. For Sub-Region II^a , however, $\mathcal{I}^{\text{util}}(-z_i) \gtrless \mathcal{I}^{\text{util}}(-z_{i'})$ and $\mathcal{I}_{\text{IP}}^{\text{util}}(-z_i) > \mathcal{I}_{\text{IP}}^{\text{util}}(-z_{i'})$, thus the order-consistency partially holds. While samples in Sub-Region II^a are jointly recognized by $\mathcal{I}^{\text{util}}$ and $\mathcal{I}_{\text{IP}}^{\text{util}}$ as detrimental, there is little practical difference.
- **(I, III).** For a case where z_i has gradients in Region I and $z_{i'}$ has gradients in Region III, $\mathcal{I}^{\text{util}}(-z_i) > \mathcal{I}^{\text{util}}(-z_{i'})$ and $\mathcal{I}_{\text{IP}}^{\text{util}}(-z_i) > \mathcal{I}_{\text{IP}}^{\text{util}}(-z_{i'})$, therefore the order-consistency holds.
- **(II, IV).** For a case where z_i has gradients in Region II and $z_{i'}$ has gradients in Region IV, the order-consistency partially holds.
- **(II, II).** For a case where both z_i and $z_{i'}$ have gradients in Region II, $\mathcal{I}^{\text{util}}(-z_i) \gtrless \mathcal{I}^{\text{util}}(-z_{i'})$ implies $\mathcal{I}_{\text{IP}}^{\text{util}}(-z_i) \gtrless \mathcal{I}_{\text{IP}}^{\text{util}}(-z_{i'})$, the order-consistency holds.

Based on the symmetry in samples (z_i and $z_{i'}$) and regions (I and III, II and IV), we can get all order-consistencies in Table 3. The bold parts are discussed above, and the rest parts are from the symmetry. In all scenarios where order-consistency does not hold, samples are jointly recognized by both $\mathcal{I}^{\text{util}}$ and $\mathcal{I}_{\text{IP}}^{\text{util}}$ as either beneficial or detrimental, resulting in minimal practical difference.

Table 3: Order-consistency in different scenarios

Gradient of z_i	Gradient of $z_{i'}$	Order-Consistency
Region I	Region I	Not Hold
Region I	Region II, IV	Partially Hold
Region I	Region III	Hold
Region II	Region I, III, IV	Partially Hold
Region II	Region II	Hold
Region III	Region III	Not Hold
Region III	Region II, IV	Partially Hold
Region III	Region I	Hold
Region IV	Region I, II, III	Partially Hold
Region IV	Region IV	Hold

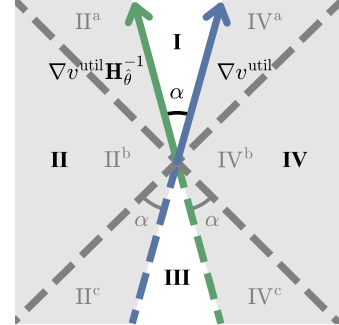


Figure 7: Visualization of the directions $\nabla v^{\text{util}} \mathbf{H}_{\hat{\theta}}^{-1}$ and ∇v^{util} .

B Detailed Information on Datasets and Model Training

We describe dataset details, model training, and other information used in the main paper, below.

B.1 Datasets

We cover our generated synthetic datasets in Section 4, vision datasets in Section 5, text datasets in Section 6, and the datasets for robustness in Section 7.

B.1.1 Synthetic Datasets

We generate two synthetic datasets to validate the correctness of our IP method in measuring the convex and non-convex models' utility, fairness, and robustness. Specifically, we generate a linear dataset using the scikit-learn library's

`make_blobs` function,³ which consists of 150 training samples and 100 test samples. The second dataset is the non-linear *half moons* dataset so that we can train a Multi-Layer Perception network with two hidden layers with ReLU activations. The training set has 250 samples and the test set has 100 samples, and the dataset is generated using the scikit-learn library’s `make_moons` function.⁴ Here we manually flip the labels of 20 samples (10 from each class) to add noise to the data.

B.1.2 Vision Datasets

Both the *CIFAR-10N* and *CIFAR-100N* datasets [59] consist of the same input images that make up the *CIFAR-10* (10 classes) and *CIFAR-100* (100 classes) datasets [48], respectively. Each input is a 32x32 RGB image with a dimension of (3,32,32). However, for *CIFAR-10N* and *CIFAR-100N*, the labels are noisy, as they contain real-world human annotation errors collected using 3 annotators on Amazon Mechanical Turk. As these datasets are based on human-annotated noise, they model noisy real-world datasets more realistically, compared to synthetic data alternatives. The training set for both datasets contains 50000 image-label pairs, and the test set contains 10000 image-label pairs that are free from noise. For *CIFAR-10N* we utilize three noise settings for experiments in the paper— (1) *Worst*, which is the dataset version with the highest noise rate (40.21%) as the worst possible annotation label for the image is chosen, (2) *Aggregate*, which is the least noisy dataset (9.03%) as labels are chosen via majority voting amongst the annotations, and (3) *Random* which has intermediate noise (17.23%) and consists of picking one of the annotators’ labels. We use the first annotator for the random labels. For *CIFAR-100N* there is only a single noisy setting (*Noisy100*) due to the large number of labeling classes, and the overall noise rate is 40.20%.

B.1.3 NLP Datasets

For the three GLUE datasets—*RTE*, *CoLA*, and *QNLI*[51], we perturbed the validation set as follows. The *Recognizing Textual Entailment* (*RTE*) dataset consists of sentence pairs labeled as entailment or not entailment. It is derived from a series of annual textual entailment challenges. The dataset includes 2,490 training examples and 277 validation examples. Since the test set does not have labels, we split the validation set into two parts, with one half used as the validation set for computing influence, and the other half used as the test set. Subsequently, we generated perturbed datasets for both the validation set and the test set using a seq2seq model [53]. The *Corpus of Linguistic Acceptability* (*CoLA*) dataset consists of sentences labeled as grammatically acceptable or unacceptable. This dataset is derived from publications in linguistics and includes 8,551 training examples and 1,043 validation examples. As with *RTE*, the test set for *CoLA* does not have labels, so we split the validation set into two parts, using one half as the validation set for computing influence, and the other half as the test set. Perturbed datasets were generated using a seq2seq model [53] for both the validation set and the test set. The *Question Natural Language Inference* (*QNLI*) dataset is a large-scale corpus for question answering, consisting of question-sentence pairs from the Stanford Question Answering Dataset (SQuAD). The task is to determine whether the context sentence contains the answer to the question. It includes 104,743 training examples and 5,463 validation examples. Similar to the other datasets, the test set does not have labels, so we split the validation set into two parts, using one half as the validation set for computing influence, and the other half as the test set. Perturbed datasets were also generated using a seq2seq model [53] for both the validation set and the test set. These datasets represent diverse natural language understanding tasks, and using them for fine-tuning helps evaluate the fairness and utility of the fine-tuned RoBERTa model.

B.1.4 Datasets for Defencing Attacks

We utilize three datasets: *Bank*, *CelebA*, and *JigsawToxicity*, to evaluate the defense against adaptive evasion adversaries using a Logistic Regression model. The *Bank* dataset [56] consists of features extracted from direct marketing campaigns of a Portuguese banking institution. The goal is to predict whether a client will subscribe to a term deposit. The dataset includes 18,292 training examples, 6,098 validation examples, and 6,098 test examples. The feature dimension of the dataset is 51. Both the validation and test sets have labels. The *CelebA* dataset [57] is a large-scale face attributes dataset with more than 200,000 celebrity images, each annotated with 40 binary attributes. For this experiment, we focus on a subset of these images. The dataset is split into 62,497 training examples, 20,833 validation examples, and 20,833 test examples. The feature dimension of the dataset is 39. Both the validation and test sets have labels. The *JigsawToxicity* dataset [58] contains a large number of comments from Wikipedia labeled for toxicity. The goal is to predict the toxicity level of a given comment. The dataset includes 18,000 training examples, 6,000 validation examples, and 6,000 test examples. The feature dimension of the dataset is 385. These datasets cover a range of tasks from marketing prediction and face attribute recognition to toxicity detection, providing a robust evaluation of the model’s defense mechanisms against adaptive adversaries.

³https://scikit-learn.org/stable/modules/generated/sklearn.datasets.make_blobs.html

⁴https://scikit-learn.org/stable/modules/generated/sklearn.datasets.make_moons.html

B.2 Models and Methods

We now describe the models and the methods used in our experiments throughout the main paper. First, we describe the ResNet-34 [50] architecture used as the base model for the noisy vision datasets, then the RoBERTa [52] NLP transformer model. We also describe implementation details and parameter values for the label correction baselines used in Sections 7 the influence-based baselines used throughout the paper.

B.2.1 MLP

In our experiments (as described in Section 4), we utilized a three-layer Multi-Layer Perceptron (MLP) classifier. This MLP is structured with three fully connected layers, each followed by a ReLU activation function. Specifically, the input layer maps the input features to 32 neurons, the hidden layer maintains this dimensionality, and the output layer is a single neuron producing the final prediction. The final layer’s output is passed through a sigmoid activation function to yield a probability score.

B.2.2 ResNet-34

The ResNet-34 model in Section 5 was proposed in [50] and is a 34-layer convolutional neural network pretrained on the ImageNet-1K dataset at resolution 224×224 . The pretrained model block is fine-tuned on the *CIFAR-10N/CIFAR-100N* training set experiments with default parameters— minibatch size (128), optimizer (SGD), initial learning rate (0.1), momentum (0.9), weight decay (0.0005), and number of epochs (100), for all experiments.

B.2.3 RoBERTa

We use the Roberta-base model from Huggingface⁵ in Section 6. A learning rate of 0.00001 and the batch sizes of *RTE*, *CoLA*, and *QNLI* are 64, 16, and 32. The model is fine-tuned over 10 epochs. The loss function used is a negative log-likelihood as the datasets are all for binary classification.

B.2.4 Logistic Regression

The Logistic Regression model in Section 7 is implemented using the `sklearn` library. The model uses L2 regularization with and a maximum iteration limit of 2048 [2].

B.2.5 Influence-Based Baselines

In our experiments, we utilize the following influence function-based methods as baselines: TracIn [16] replaces the Hessian matrix with the identity matrix; LiSSA [10] and EKFAC [13] use implicit Hessian-vector products and Kronecker-Factored curvature to efficiently approximate the inverse of the Hessian matrix; DataInf [3] swaps the order of matrix multiplication to obtain a closed-form expression; Self-TracIn [18] and Self-LiSSA [17] are self-expression versions of TracIn and LiSSA, where ∇v^{util} is replaced with $\nabla_{\hat{\theta}} \ell(z_i; \hat{\theta})$. Our IP closely resembles TracIn, with the added application of dropout with $\mathcal{U}(0, 0.01)$ on the model parameters. Additionally, our IP Ensemble constitutes an ensemble version of IP with an ensemble size of 5.

C Additional Experimental Results and Analysis

C.1 IP for measuring fairness and robustness

Similar to Figure 2, we conduct the experiments based on Eqs. (3) and (4) to demonstrate the effectiveness of our IP in measuring the sample influence on fairness and robustness. Figure 8 shows the relationship between IP and the traditional influence function, indicating IP is a good surrogate of the traditional influence function in measuring fairness and robustness as well.

C.2 Performance of IP Ensemble with different rates of removed samples

In our paper, we explore different rates of removed samples on *CIFAR-10N-a*. Table 4 shows the performance of IP Ensemble with different rates of removed samples. Except for not removing, there is no significant difference in the remaining results.

⁵https://huggingface.co/docs/transformers/model_doc/roberta

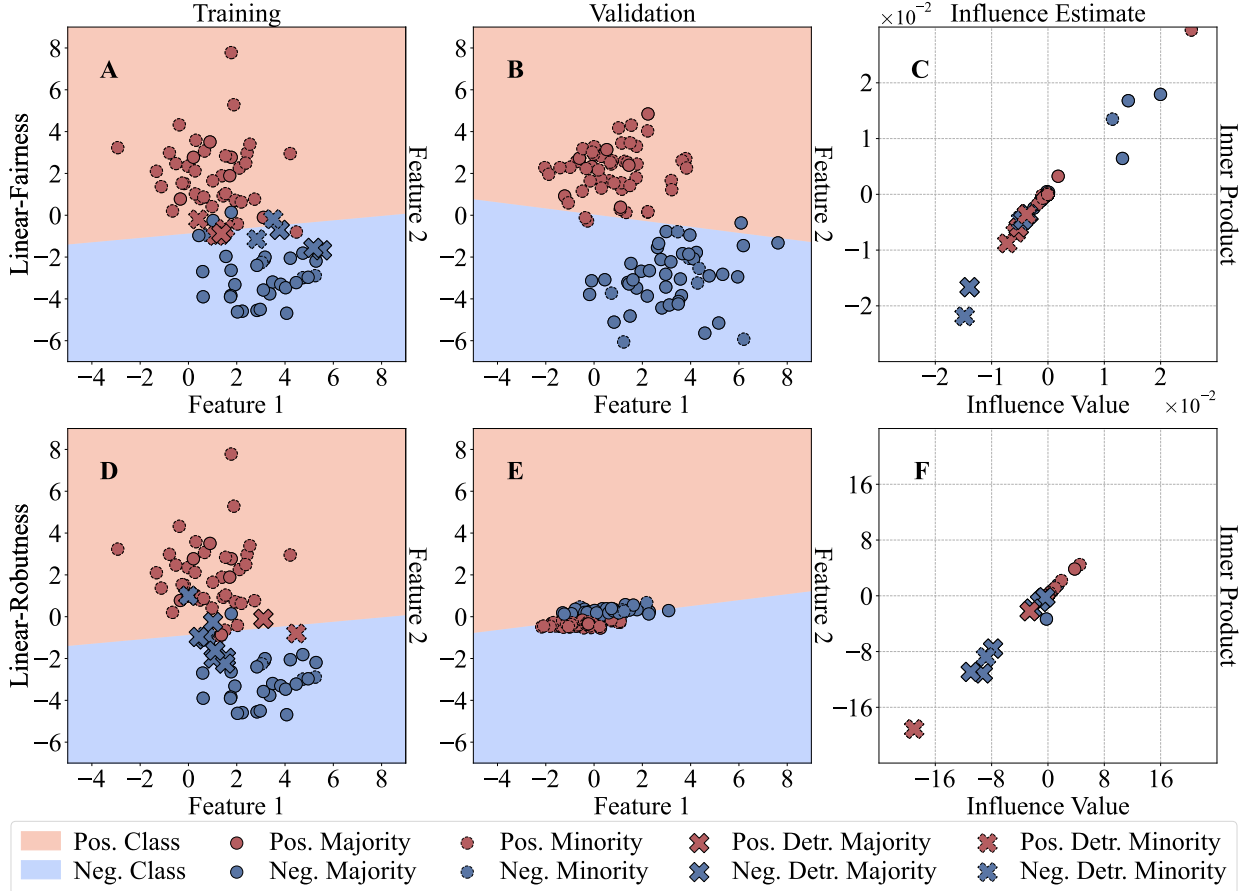


Figure 8: Illustrating our inner product approach on measuring fairness and robustness. **A** and **D** illustrate the same 2D linearly separable synthetic dataset in Figure 2 trained using a Logistic Regression model for binary classification, where the solid and dashed point boundaries denote the majority and minority subgroups. **B** and **E** represent the validation set. **C** and **F** show the estimated influence on fairness and robustness by the traditional influence function and our IP method.

Table 4: Performance of IP Ensemble with different rates of removed samples on *CIFAR-10N-a*

Method	Ensemble Size	Remove Rate	ACC
Cross Entropy	5	0	91.62
IP Ensemble (Ours)	5	0.025	92.29 ± 0.16
IP Ensemble (Ours)	5	0.050	92.26 ± 0.19
IP Ensemble (Ours)	5	0.075	92.50 ± 0.13
IP Ensemble (Ours)	5	0.100	92.37 ± 0.15

C.3 Parameter Analysis on Dropout Rate and Ensemble Size

Table 5 shows the performance of different dropout rates and ensemble sizes of IP Ensemble. As can be observed, our IP Ensemble is not sensitive to dropout rate, and its performance increases with a large ensemble size, demonstrating the effectiveness of the ensemble strategy. It is also worth noting that although our IP Ensemble runs fast, it might take a longer time to calculate the sample gradient.

Table 5: Performance of different dropout rate and ensemble size of IP Ensemble on *CIFAR-10N-a*, *CIFAR-10N-r*, *CIFAR-10N-w*, and *CIFAR-100N*

Ensemble Size	Dropout Rate	<i>CIFAR-10N-a</i>	<i>CIFAR-10N-r</i>	<i>CIFAR-10N-w</i>	<i>CIFAR-100N</i>
5	0.01	92.26 ± 0.19	91.28 ± 0.29	86.50 ± 0.35	62.25 ± 0.54
5	0.1	92.26 ± 0.19	91.28 ± 0.29	86.50 ± 0.35	62.25 ± 0.54
5	0.5	92.26 ± 0.19	91.28 ± 0.29	86.50 ± 0.35	62.25 ± 0.54
1	0.01	92.42 ± 0.17	90.82 ± 0.08	86.31 ± 0.35	60.59 ± 0.20
5	0.01	92.26 ± 0.19	91.28 ± 0.29	86.50 ± 0.35	62.25 ± 0.54
10	0.01	92.58 ± 0.04	91.32 ± 0.29	86.89 ± 0.37	61.82 ± 0.61
15	0.01	92.27 ± 0.09	91.27 ± 0.28	86.47 ± 0.41	61.59 ± 0.34
20	0.01	92.41 ± 0.15	91.33 ± 0.26	86.65 ± 0.16	62.25 ± 0.11

C.4 Time Complexity and Execution Time of Various Influence Function-based Methods on Vision Datasets

Table 6 shows the time complexity of various influence function-based methods. Except for the vanilla calculation, all other methods have linear time complexity in terms of the sample size. However, they have large divergence in real execution time.

Table 6: Computational complexity of various influence-function-based methods (n is #training samples and p is #model parameters, k is #ensemble size. “-” denotes no runs.)

Method	Type	Time Complexity	<i>CIFAR-10N</i>	<i>CIFAR-100N</i>	<i>Animal-10N</i>
Exact by Eq. (1)	Hessian-based	$\mathcal{O}(np^3)$	-	-	-
TracIn [16]	Hessian-free	$\mathcal{O}(np)$	0.03	0.28	0.03
LiSSA [10]	Hessian-based	$\mathcal{O}(np)$	7.67	34.59	7.46
EKFAC [13]	Hessian-based	$\mathcal{O}(np^2)$	22.54	192.58	23.89
DataInf [3]	Hessian-based	$\mathcal{O}(np)$	11.50	45.29	10.89
Self-TracIn [18]	Self-influence	$\mathcal{O}(np)$	0.15	1.41	0.15
Self-LiSSA [17]	Self-influence	$\mathcal{O}(np)$	14.57	54.39	14.40
IP Ensemble (Ours)	Hessian-free	$\mathcal{O}(npk)$	0.03	0.28	0.03

We omit the specific timing details for the sample gradient, which are readily available during the base model’s training phase. Besides, utilizing vmap in Pytorch, we can efficiently compute gradients in parallel. For example, in Section 5, it only takes 61 seconds and 4 seconds to calculate ∇v^{util} and $\nabla_{\hat{\theta}} \ell(z_i; \hat{\theta})$ on *CIFAR-10N* dataset, respectively.

D Broader Impact and Limitations

Our work aims to address issues that currently hinder the applicability of influence estimation in deep learning models. By enabling influence estimation for deep models, practitioners can assess whether training samples are beneficial or detrimental to performance, making models more interpretable and performant. As we demonstrate through extensive experiments across multiple problem settings, our proposed outlier gradient analysis approach outperforms existing baselines and can augment model performance by trimming detrimental samples. As a result, our work paves the way for significant positive societal impact, especially with the increased adoption of larger and deeper neural networks such as LLMs. However, despite our research demonstrating superior performance and potential benefits, there are several limitations to consider. First, the simplicity of our Hessian-free approximation method, while effective in many scenarios, may not capture the full complexity of more nuanced model behaviors and interactions within the data. Additionally, our method assumes a level of model and data homogeneity that might not hold in highly heterogeneous datasets or more complex model architectures. Furthermore, while our IP Ensemble strategy enhances generalization by simulating diverse models, it introduces additional computational overhead and complexity that may not be feasible for all applications or environments, particularly those with limited computational resources. There is also the consideration of robustness and fairness across different domains and types of data; our current evaluations, while extensive, may not cover all possible scenarios or edge cases, potentially limiting the generalizability of our findings. Finally, ethical considerations around data trimming and sample selection must be carefully managed to avoid unintended biases or negative impacts on model performance for underrepresented groups. As influence estimation becomes more integrated

into model training and evaluation pipelines, ongoing research and monitoring will be essential to ensure that these techniques are applied responsibly and equitably.

E Code and Reproducibility

We will release the code soon.